www.neurosci.cn
www.springer.com/12264

ORIGINAL ARTICLE

Prestin-Mediated Frequency Selectivity Does not Cover Ultrahigh Frequencies in Mice

Jie Li[1,2] · Shuang Liu[1,2] · Chenmeng Song[1,2] · Tong Zhu[1,2] · Zhikai Zhao[1,2] ·
Wenzhi Sun[3,4] · Yi Wang[1,2] · Lei Song[5,6,7] · Wei Xiong[1,2]

Abstract In mammals, the piezoelectric protein, Prestin, endows the outer hair cells (OHCs) with electromotility (eM), which confers the capacity to change cellular length in response to alterations in membrane potential. Together with basilar membrane resonance and possible stereociliary motility, Prestin-based OHC eM lays the foundation for enhancing cochlear sensitivity and frequency selectivity.

Jie Li, Shuang Liu, and Chenmeng Song contributed equally to this work.

✉ Yi Wang
   yiwang2020@tsinghua.edu.cn

✉ Lei Song
   lei.song@yale.edu

✉ Wei Xiong
   wei_xiong@tsinghua.edu.cn

1   School of Life Sciences, Tsinghua University, Beijing 100084, China

2   IDG/McGovern Institute for Brain Research at Tsinghua University, Tsinghua University, Beijing 100084, China

3   Chinese Institute for Brain Research, Beijing 102206, China

4   School of Basic Medical Sciences, Capital Medical University, Beijing 100069, China

5   Department of Otolaryngology, Head and Neck Surgery, Shanghai Ninth People's Hospital, Shanghai Jiao Tong University School of Medicine, Shanghai 200011, China

6   Ear Institute, Shanghai Jiao Tong University School of Medicine, Shanghai 200092, China

7   Shanghai Key Laboratory of Translational Medicine on Ear and Nose Diseases, Shanghai 200011, China

However, it remains debatable whether Prestin contributes to ultrahigh-frequency hearing due to the intrinsic nature of the cell's low-pass features. The low-pass property of mouse OHC eM is based on the finding that eM magnitude dissipates within the frequency bandwidth of human speech. In this study, we examined the role of Prestin in sensing broad-range frequencies (4–80 kHz) in mice that use ultrasonic hearing and vocalization (to >100 kHz) for social communication. The audiometric measurements in mice showed that ablation of Prestin did not abolish hearing at frequencies >40 kHz. Acoustic associative behavior tests confirmed that *Prestin*-knockout mice can learn ultrahigh-frequency sound-coupled tasks, similar to control mice. *Ex vivo* cochlear Ca^{2+} imaging experiments demonstrated that without Prestin, the OHCs still exhibit ultrahigh-frequency transduction, which in contrast, can be abolished by a universal cation channel blocker, Gadolinium. *In vivo* salicylate treatment disrupts hearing at frequencies <40 kHz but not ultrahigh-frequency hearing. By pharmacogenetic manipulation, we showed that specific ablation of the OHCs largely abolished hearing at frequencies >40 kHz. These findings demonstrate that cochlear OHCs are the target cells that support ultrahigh-frequency transduction, which does not require Prestin.

Introduction

Mammalian auditory function has ample capacity to discriminate sound frequencies ranging from several Hz to >100 kHz [1]. In large part, this functionality relies on the organ of Corti, a relatively newly-evolved organ

comparable to that found in lower vertebrates, which is comprised of three rows of outer hair cells (OHCs) and one row of inner hair cells (IHCs). The frequency-selectivity of hair cells is determined by their position along the cochlear coil. At the apex, the hair cells sense low frequencies; at the basal turn, they detect high frequencies [2, 3]. At each frequency, a travelling wave vibrates on the basilar membrane and finds its best matching position where OHCs actively and locally amplify the motion between the tectorial and basilar membranes [2, 4]. OHCs can change their length in response to fluctuations in receptor potential, a property also defined as electromotility (eM) [5–8]. OHC-based eM is believed to contribute to cochlear amplification, which significantly improves hearing sensitivity and frequency-selectivity in mammals [2, 3].

The somatic eM of the OHC is generated by the motor protein, Prestin [2, 9, 10]. As it is extensively expressed on the lateral membrane of OHCs, Prestin behaves as a biological piezoelectric element containing at least two functional domains: a voltage sensor, which detects fluctuations in membrane potential, and an actuator, which can undergo conformational change [10–12]. Recently, these component domains have been depicted by cryoelectron microscopy as discrete structures [13–15]. Prestin is the key protein enhancing the frequency-tuning process by providing OHCs with eM that is the basic mechanism driving cochlear amplification [10, 16, 17].

Although active cochlear amplification has been recorded both *in vivo* and *in vitro* at wide-ranging frequencies, the contribution of Prestin-based somatic eM at high frequencies remains elusive. In order to generate cochlear amplification, the OHC must change its length in a cycle-by-cycle manner, as reported at lower frequencies, such as 1 kHz [4, 9]. However, theoretically, Prestin-driven amplification is limited by two low-pass filters: one is formed by the resistance and capacitance of the cell membrane [18] and the other is due to the internal limitations in the velocity of conformational change of Prestin [19]. Using different recording configurations, the measured cut-off frequency of OHC eM varies considerably across several studies, in which the upper limit ranged from a few kHz [20] to at least 79 kHz [21–23]. Thus, whether Prestin-based OHC motility can power amplification through ultrahigh frequencies has not yet been established.

Interestingly, many animals, including mice, use ultrasonic hearing and vocalization (20 kHz to >100 kHz) for communication [24]. Previous phylogenetic and functional studies on Prestin have revealed trends in the distribution of genetic polymorphisms that appear to coincide with the ability of particular species to echolocate [25–29]. This suggests a co-evolution of Prestin eM with the ultrasonic vocalization of echolocating animals, such as cetaceans,

bats, and dolphins. Also noteworthy, *in vivo* approaches have shown that Prestin enhances hearing sensitivity across the whole frequency range [16, 30]. On the other hand, our recent study revealed that PIEZO2, a mechanically-activated channel, likely mediates ultrasonic hearing *via* OHCs [31]. Taken together, these data have motivated further study of the essential role Prestin plays in ultrasonic hearing.

Materials and Methods

Mouse Strains and Animal Care

Prestin-knockout (*Prestin*-KO) and *Prestin-P2A-DTR* (diphtheria toxin receptor) (*Prestin*-DTR) mouse lines were generated as described [32, 33]. Wild-type (WT) C57BL6 (B6) mice were used as controls for *Prestin*-KO mice. *Prestin*-DTR and littermate controls at the age of 3 weeks received a single intraperitoneal (i.p.) injection of diphtheria toxin (DT; Sigma, 2 μg/mL dissolved in saline) at a dose of 20 ng/g body weight. One week later, foot-shock behavior and audiometry were recorded in both DTR and littermate mice. The experimental procedures were approved by the Institutional Animal Care and Use Committee of Tsinghua University.

Modified Auditory Brainstem Response (mABR)

Mice of either sex were anesthetized with 0.4% pentobarbital sodium in saline (0.2 mL/10 g, volume/body weight, i.p.). During the whole experiment, body temperature was maintained at 37 °C by a heating pad. After vertex skin removal, the skull was exposed and secured with a stainless-steel screw (M1.4 × 2.5). In contrast to the classical ABR configuration, a modified ABR (mABR) configuration was recorded to acquire better ABRs in response to ultrahigh-frequency stimuli. This was accomplished by connecting the electrode to a microscrew attached to the skull posterior to bregma (–7 mm AP, 0 mm ML), as previously described [31]. Precautions were taken not to puncture the dura. A recording electrode was connected to the screw by a silver wire with a diameter of 0.1 mm. Other operations were similar to regular ABR procedures. Reference and ground electrodes were inserted subcutaneously at the pinna and groin, respectively. The animals were overdosed with pentobarbital at the end of acute experiments. In survival experiments, the screw was secured with dental cement for later measurements. After surgery, lidocaine ointment was applied locally and Meloxicam (4 mg/kg i.p.) was injected for anesthesia, analgesia, and anti-inflammation.

mABR data were collected at ∼200 kHz by an RZ6 workstation controlled by BioSig software (Tucker-Davis

Technologies, Alachua, FL). Clicks and 4–16 kHz pure-tone bursts were generated by a TDT MF1 closed-field magnetic speaker. A TDT EC1 (Coupler Model) electrostatic speaker was used to generate high frequencies (32–80 kHz). Prior to experiments, the two speakers were calibrated using 377C01 (free-field) or 377C10 (pressure) microphones with a 426B03 preamplifier and a 480C02 signal conditioner (PCB Piezotronics, Depew, NY). For sound stimulation, 0.1-ms clicks or 5-ms tone-bursts with a 0.5-ms rise/fall time were delivered at 21 Hz, with intensities ranging from 90 to 10 dB SPL in 10-dB steps. Responses to each acoustic stimulation with defined frequency and intensity levels were bandpass filtered (100 or 300 to 3000 Hz), amplified by RA4LI & RA4PA Medusa PreAmps (Tucker-Davis Technologies, Alachua, FL), repeatedly sampled 512 times, and then averaged. For lower frequencies, the lowest stimulus sound level at which a repeatable wave I could be identified was defined as the threshold [34]. Typically, frequencies >54 kHz in waveform were hard to identify due to the low signal-to-noise ratio. In most cases, wave I was missing in the waveform as reported by other groups [35]. However, one peak appeared at ∼3 ms and its latency increased and amplitude decreased with stimulus levels. This peak was used to identify the threshold when wave I could not be detected. The responses disappeared postmortem, so the signals were biological.

Salicylate, a known competitor of intracellular chloride binding, was used to inhibit the functionality of Prestin. Specifically, 200 mg/kg sodium salicylate was applied i.p. to 1-month-old WT B6 mice. A higher salicylate dose was avoided since it can induce higher hearing-threshold elevation, making survival more difficult for mice during the 2-h measurement sessions. The 200 mg/kg limit introduced only mild hearing threshold elevation at lower frequencies by ∼20 dB SPL. mABR thresholds were monitored every 10 min until 120 min post-injection and were measured again on day 2 to record the recovery. For finer time resolution, the responses were averaged 256 times, and only the EC1 speaker was used to deliver the pure tone stimuli (12–80 kHz) in a close-field configuration. Each measurement took ∼8 min.

Acoustic Cue-Associated Freezing Behavior

Male mice were used to investigate freezing behavior. Mouse locomotion in an operant (cubic, 30 × 30 × 30 cm^3) or activity box (cylindrical, diameter of 35 cm and height 30 cm) was carried out in a soundproof chamber (Shino Acoustic Equipment Co., Ltd, Shanghai, China), and captured on camera with an infrared light source. Each mouse was allowed to freely explore the operant box for 30 min before the sound-associated foot-shock training.

During the training, an acoustic cue of 10 s containing a 50-ms pure tone (16 kHz or 63 kHz) at 50-ms intervals, was played. Electrical shocks of 1 s at 0.6 mA were given to the mouse at 5 s and 10 s. In the operant box, the electrical shocks were delivered by a metal grid floor powered by an electrical stimulator (YC-2, Chengdu Instrument Inc., Chengdu, China). Acoustic cues were generated by a free-field electrostatic speaker ES1 placed 15 cm above the floor and powered by an RZ6 workstation with BioSig software (Tucker-Davis Technologies, Alachua, FL). The cue was delivered every 3 min, and repeated 10 times before the trained mouse was placed into the home cage. After 24 h, the trained mouse was transferred to an activity box to test freezing behavior. In the activity box, the same ES1 speaker was placed 15 cm above the chamber floor to generate a 16 kHz or 63 kHz acoustic cue of 10 s duration (identical to the training cues). Cues were delivered at least 5 times during each test procedure. The sound intensity on the arena floor was calibrated from 70 dB SPL to 90 dB SPL, which is in the range of mouse hearing.

Immunostaining

Mice were selected for immunostaining at the ages of 3 weeks, 1 month, 6 weeks, or 2 months. After anesthesia with Avertin (30 mg/mL in saline, 0.12–0.15 mL/10 g), mice were perfused with ice-cold phosphate-buffered saline (PBS), and then sacrificed by decapitation. The inner ears were dissected from the temporal bone, and fixed in fresh 4% paraformaldehyde (DF0135, Leagene, Anhui, China) in PBS for 12–24 h at 4 °C. After fixation, the inner ears were washed three times (10 min each) with PBS, and then immersed in 120 mM EDTA decalcifying solution (pH 7.5) for 24 h at room temperature (RT, 20–25 °C). This step was also followed by PBS washing.

The cochlear coils were finely dissected from the inner ears in PBS and blocked in 1% PBST [PBS + 1% Triton X-100 (T8787, Sigma-Aldrich, St. Louis, MO)] with 5% BSA (A3059, Sigma-Aldrich, St. Louis, MO) at room temperature for 1 h. The cochlear tissue was then incubated in 0.1% PBST/5% BSA solution with MYO7A antibody (1:1000, Cat.25-6790, Proteus Biosciences Inc., Ramona, CA) overnight at 4 °C and washed 3 times with 0.1% PBST at RT. The tissue was incubated with secondary antibody (Invitrogen anti-rabbit Alexa Fluor 647, 1:1000, A21244; Invitrogen Alexa Fluor 488 Phalloidin, 1:1000, Cat. A12379) and 1:1000 DAPI in 0.1% PBST/5% BSA solution at RT for 2–4 h. The tissue was washed 3 times with 0.1% PBST and mounted with ProLong Gold Antifade Mountant (Cat. P36930, Life Technology, Rockville, MD). Fluorescent immunostaining patterns were captured by an A1/SIM/STORM confocal microscope (A1

N-SIM STORM, Nikon, Japan). Whole-view images of cochlear tissue were composited using Photoshop software (Adobe, San Jose, CA).

Cochlear Ca²⁺ Imaging

A hemicochlear preparation [36, 37] was used for Ca^{2+} imaging of OHCs [31]. Mice at 1 month of age were anesthetized with isoflurane and sacrificed, and then the cochleae were dissected out using a dissection solution containing (in mmol/L): 5.36 KCl, 141.7 NaCl, 1 $MgCl_2$, 0.5 $MgSO_4$, 0.1 $CaCl_2$, 10 H-HEPES, 3.4 L-glutamine, 10 D-glucose (pH 7.4, osmolarity 290 mmol/kg). After immersion in cutting solution containing (in mmol/L) 145 NMDG-Cl, 0.1 $CaCl_2$, 10 H-HEPES, 3.4 L-glutamine, 10 D-glucose (pH 7.4, osmolarity 290 mmol/kg), cochleae were glued to a metal block with Loctite 401 and cut into 2 halves by a vibratome (VT1200S, Leica, Wetzlar, Germany; FREQ index at 7/Speed index at 50). The section plane was configured in parallel to the modiolus to minimize tissue damage. The hemicochleae were transferred into a recording dish, glued to the bottom, and loaded with 25 μg/mL Fluo-8 AM (Invitrogen, Waltham, MA) in the recording solution. After 10-min incubation in a dark box at RT, the dye-loading solution was replaced by dye-free recording solution containing (in mmol/L): 144 NaCl, 0.7 Na_2PO_4, 5.8 KCl, 1.3 $CaCl_2$, 0.9 $MgCl_2$, 10 H-HEPES, 5.6 D-glucose (pH 7.4, osmolarity 310 mmol/kg).

An upright microscope (BX51WI, Olympus, Tokyo, Japan) equipped with a 60× water immersion objective (LUMPlanFL, Olympus, Tokyo, Japan) and an sCMOS camera (ORCA Flash 4.0, Hamamatsu, Hamamatsu-Shi, Japan) was used for Ca^{2+} imaging, controlled by MicroManager 1.6 software [38] with a configuration of 4 × 4 binning, 100-ms exposure time, and 2-s sampling interval. To maintain the best performance of the hemicochlea preparations, the whole procedure from cutting to imaging was finished within 15 min to ensure tissue sample integrity.

Ultrasound Generation and Delivery *ex vivo*

A customized 80-kHz ultrasound transducer 27 mm in diameter was powered by a radio-frequency amplifier (Aigtek, ATA-4052, China) integrated with a high-frequency function generator (Rigol, DG1022U, China). An 80-kHz transducer was chosen because of its relatively small size (the lower the frequency, the larger the size) and its compatibility with physiological hearing frequencies in mice. For calibration, a high-sensitivity hydrophone (Precision Acoustics, UK) was positioned directly above the vibration surface. Transducer outputs were calibrated in a

tank filled with deionized, degassed water under free-field conditions. To stimulate the cochlea, the transducer was tightly fixed to the bottom of the recording dish with ultrasound gel. The distance between the tissue and ultrasound transducer was <5 mm. For the 80-kHz ultrasonic stimulation, a single pulse of 100 ms was applied, with a calibrated intensity at 8.91 W/cm² I_SPTA.

Low-frequency Fluid-jet Stimulation of Cochlea

The fluid-jet configuration was used as previously reported [39]. Briefly, a 27-mm diameter circular piezoelectric ceramic was sealed in a self-designed mineral oil tank. An electrode with a 5–10 μm diameter tip filled with recording solution (in mmol/L: 144 NaCl, 0.7 Na_2PO_4, 5.8 KCl, 1.3 $CaCl_2$, 0.9 $MgCl_2$, 10 H-HEPES, 5.6 D-glucose, pH 7.4, osmolarity 310 mmol/kg) was mounted in the tank and transmitted the pressure wave to the hair bundle of an OHC in cochlea samples. The circular piezoelectric ceramic was driven by a sinusoidal voltage fluctuation generated from a patch-clamp amplifier (EPC10 USB, HEKA Elektronik, Lambrecht/Pfalz, Germany) and amplified 20-fold with a custom high-voltage amplifier. The 100-ms sinusoidal stimulation was delivered at a frequency of 2000 Hz and an amplitude of 130 V.

Nonlinear Capacitance Recording

Neonatal mice at P7–P8 were used. Basilar membrane with hair cells was dissected and bathed in external solution containing (in mmol/L): 120 NaCl, 20 TEA-Cl, 2 $MgCl_2$, 2 $CoCl_2$, and 10 H-HEPES (pH 7.3 with NaOH, osmolality 300 mmol/kg with D-glucose). An internal solution at the same pH and osmolality contained (in mmol/L): 140 CsCl, 2 $MgCl_2$, 10 EGTA, and 10 H-HEPES. Whole-cell patch clamping was done at a holding potential of 0 mV (Axon Axopatch 200B, Molecular Devices, Sunnyvale, CA). A continuous high-resolution two-sine stimulus (390.6 and 781.2 Hz) with 10 mV peak amplitude superimposed on a 250-ms voltage ramp (from +150 to –150 mV) was used. Data were acquired and analyzed using jClamp (Scisoft, New Haven, CT). Capacitance-voltage data were fit with a two-state Boltzmann function.

$$C_m = NLC + C_{lin} = Q_{max} \frac{ze}{k_B T} \frac{b}{(1+b)^2} + C_{lin}$$

where

$$b = \exp\left(-ze \frac{V_m - V_h}{k_B T}\right)$$

C_{lin} is the linear membrane capacitance, Q_{max} is the maximum nonlinear charge, z is valence, e is electron

charge, K_B is the Boltzmann constant, T is absolute temperature, V_m is membrane potential, and V_h is voltage at peak capacitance.

Experimental Design and Statistical Analysis

For animal tracing and locomotion evaluation, videos of mouse locomotion in foot-shock were analyzed using MatLab (MathWorks, Natick, MA) and EthoVision XT software (v11.5, Noldus, Wageningen, Netherland). The center of each mouse was used to draw the locomotion trace. To show speed, the locomotion trace was dotted every 0.5 s. To analyze foot-shock behavior, the percentage freezing time pre-cue (30 s before conditioned stimulus), and post-cue (30 s after conditioned stimulus), were calculated to compare the effect of sound-induced freezing.

For Ca^{2+} data analysis, to extract fluorescence signals we visually identified the regions of interest (ROIs) based on fluorescence intensity. To estimate fluorescence changes, the pixels in each specified ROI were averaged (F). Relative fluorescence changes, $DF/F_0 = (F-F_0)/F_0$, were calculated as Ca^{2+} signals. The cochlear imaging data were analyzed offline using Micromanager software. An ROI was drawn to cover each hair cell. The fluorescence intensity of each ROI was normalized to its value in the frame immediately prior to each stimulation.

Data were managed and analyzed with MatLab 2014b (MathWorks, Natick, MA), Excel 2016 (Microsoft, Seattle, WA), Prism 6 (GraphPad Software, San Diego, CA), and Igor pro 6 (WaveMetrics, Lake Oswego, OR). N numbers are indicated in the figures or legends. For audiometry and behavioral experiments, N values present biological replicates of individual mice. For cochlear Ca^{2+} imaging experiments, N values indicate biological replicates of individual cells, which were collected from at least 3 mice. All data are shown as the mean $\pm$ SD, as indicated in the figure legends. We used a two-tailed *t*-test for one-to-one comparison or one-way ANOVA for one-to-many comparisons to determine statistical significance (*P <0.05, **P <0.01, ***P <0.001, and ****P <0.0001), which were compared by nonparametric tests if the data distribution was not Gaussian.

Results

Ultrahigh-frequency Hearing is Preserved in Mice with Prestin Knockout

In order to determine whether Prestin is crucial for ultrahigh-frequency hearing, the ABR thresholds were measured in both *Prestin*-KO and WT mice for hearing sensitivity at multiple frequencies (up to 80 kHz) (Fig. 1).

The *Prestin*-KO mouse was generated by a CRISPR/Cas9-mediated base editing approach, and showed a loss of OHC-eM [32] as previously described [17].

Consistent with previous studies [17], 2-month old *Prestin*-KO mice exhibited significantly elevated pure-tone mABR thresholds at 4–32 kHz cues; although these thresholds were relatively high ($\sim$70 dB SPL), they were still in the detectable range (Fig. 1A, E, dark purple). However, at frequencies >40 kHz, the *Prestin*-KO mice at 2 months showed mABR thresholds >90 dB SPL, the ceiling threshold indicative of profound deafness in general ABR testing (Fig. 1A, D, E, dark purple). One-month-old *Prestin*-KO mice showed mABR deficits similar to 2-month-old *Prestin*-KO mice at hearing frequencies ranging from 4 kHz to 32 kHz (Fig. 1B, E, light purple *vs* dark purple). However, hearing in the 40–80 kHz range was preserved with thresholds similar to control WT mice (Fig. 1C, D, E, light purple *vs* gray), distinct from that of 2-month-old *Prestin*-KO mice (Fig. 1D, E, light purple *vs* dark purple). The amplitude of P1–N1 of the mABR waveform in 1-month-old *Prestin*-KO mice was decreased by nearly half (Fig. S1). This implies that the *Prestin*-KO mice suffered some degree of neuronal loss prior to the elevation of mABR thresholds. Together, these results indicate that in mice, Prestin enhances hearing sensitivity primarily in an upper limit range of 40 kHz, but plays a less important role at frequencies above 40 kHz.

Freezing Behavior Associated with Ultrahigh-frequency Hearing is Preserved in Prestin-KO Mice

To confirm that Prestin-driven OHC mechanics were not crucial for ultrahigh-frequency hearing, sound-associated fear conditioning experiments were performed for low- and high-frequency hearing in *Prestin*-KO mice (Fig. 2A). In the *Prestin*-KO mice and control cohorts, fear-conditioning tests were applied using an acoustic cue that was paired with electrical shocks to generate conditioned-freezing behaviors (Fig. 2A). On day 2, 1-month-, 2-month-old *Prestin*-KO, and 1-month-old WT mice were examined for sound cue-associated freezing behavior (Fig. 2B). The 1-month-old *Prestin*-KO mice were able to be trained to respond to the 16-kHz cue at 90 dB SPL but had a limited response to this cue at 60 dB SPL, while the control WT mice responded to the 16-kHz cue at both intensities (Fig. 2B–D). This demonstrates that the cochlear amplifier is intact in WT in the low-frequency range.

By comparison, both the 1-month-old *Prestin*-KO and WT mice acquired freezing behavior in response to the 63-kHz cue at 90 dB SPL (Fig. 2B, E). Consistent with the above mABR results, *Prestin*-KO mice showed associative freezing to the 63-kHz cue at 1 month but lost this
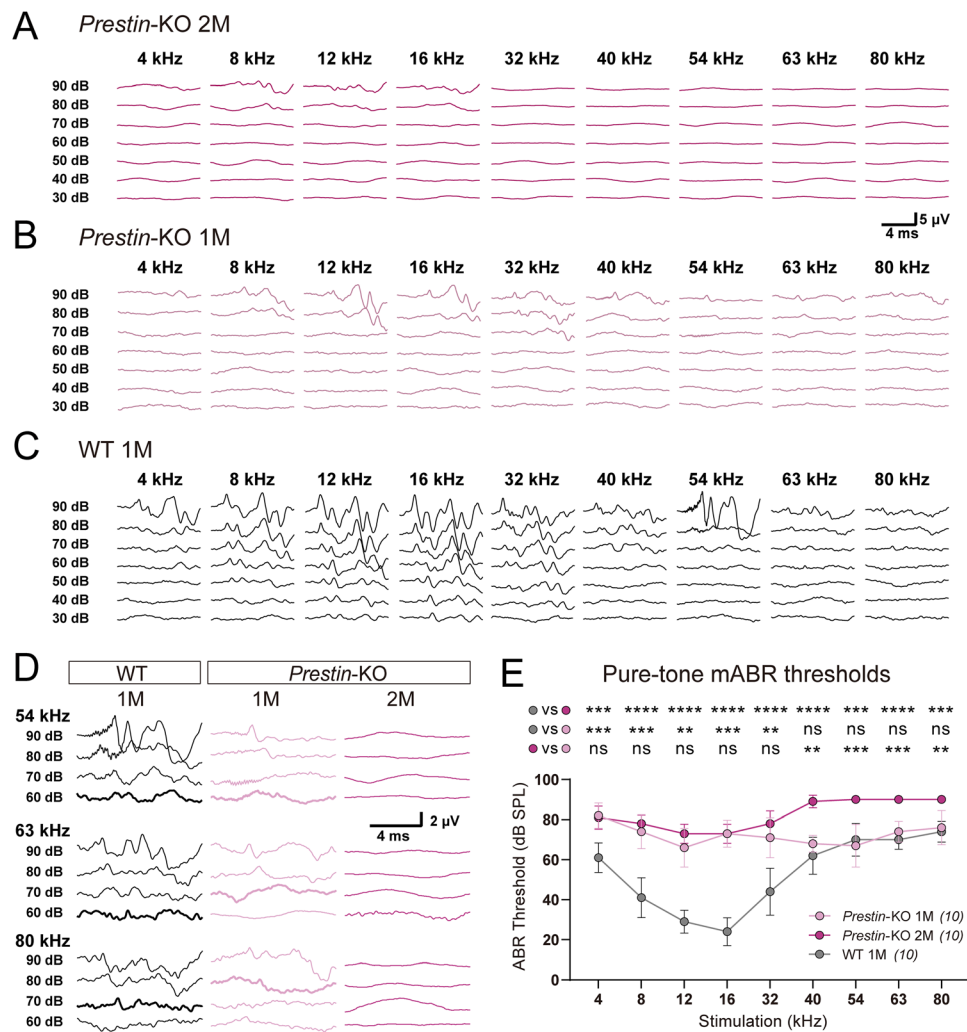
774

Neurosci. Bull. July, 2022, 38(7):769–784

Fig. 1 *Prestin*-knockout mice show distinct sensitivity at low and high frequencies. **A** Representative example of mABR signals in a 2-month-old (2M) *Prestin*-KO mouse. **B** Representative example of mABR signals in a 1-month (1M) *Prestin*-KO mouse. **C** Representative example of mABR signals in a 1-month (1M) WT C57BL/6 mouse. **D** Enlarged mABR traces with 54 kHz, 63 kHz, and 80 kHz sound stimuli in (**A**–**C**). Bold lines indicate visual thresholds. Peak at ~3 ms was used to identify the threshold for high frequencies. **E** Pure-tone mABR thresholds in *Prestin*-KO mice and control mice at designated ages. Note the distinct ABR thresholds to ultrasound frequencies between *Prestin*-KO mice at 1 month (1M, light purple) and *Prestin*-KO mice at 2 months (2M, purple). 1-month-old (1M) *Prestin*-KO mice *vs* control mice, Kruskal-Wallis test, 4 kHz, ***P = 0.0002; 8 kHz, ***P = 0.0006; 12 kHz, **P = 0.0026; 16 kHz, ***P = 0.0002; 32 kHz, **P = 0.0047; 40 kHz, P = 0.7802; 54 kHz, P >0.9999; 63 kHz, P = 0.9704; 80 kHz, P >0.9999. 2-month (2M) *Prestin*-KO mice *vs* control mice, Kruskal-Wallis test, 4 kHz, ***P = 0.0005; 54 kHz and 80 kHz, ***P = 0.0003; ****P <0.0001 at other frequencies. 1-month-old (1M) *Prestin*-KO *vs* 2-month-old (2M) *Prestin*-KO mice, Kruskal-Wallis test, 4 kHz, P >0.9999; 8 kHz, P > 0.9999; 12 kHz, P = 0.7182; 16 kHz, P >0.9999; 32 kHz, P = 0.734; 40 kHz, **P = 0.0016; 54 kHz, ***P = 0.0001; 63 kHz, ***P = 0.0009; 80 kHz, **P = 0.0013. Data are presented as the mean ± SD. N numbers are shown in panels.

sensitivity at 2 months of age (Fig. 2B–E). Freezing behavior in *Prestin*-KO mice was not as pronounced as that seen in WT mice when coupled with either 16 kHz or 63 kHz (Fig. 2C–E). This was thought to be the result of decreased freezing time potentially due to disrupted cochlear function [10, 16, 17]. These results suggest that Prestin and its eM may modestly contribute to, but are not essential for ultrahigh-frequency hearing.

Progressive Loss of Cochlear Hair Cells in *Prestin*-KO Mice

It has been reported that ablation of Prestin induces the progressive loss of hair cells [40]. Therefore, we assessed the survival of hair cells in *Prestin*-KO mice at different ages. At 2 months of age, *Prestin*-KO mice lost the majority of OHCs and some basal IHCs (Fig. 3A, D). This may explain the abolished mABR signals at ultrahigh frequencies (Fig. 1E, dark purple). The absence of hair
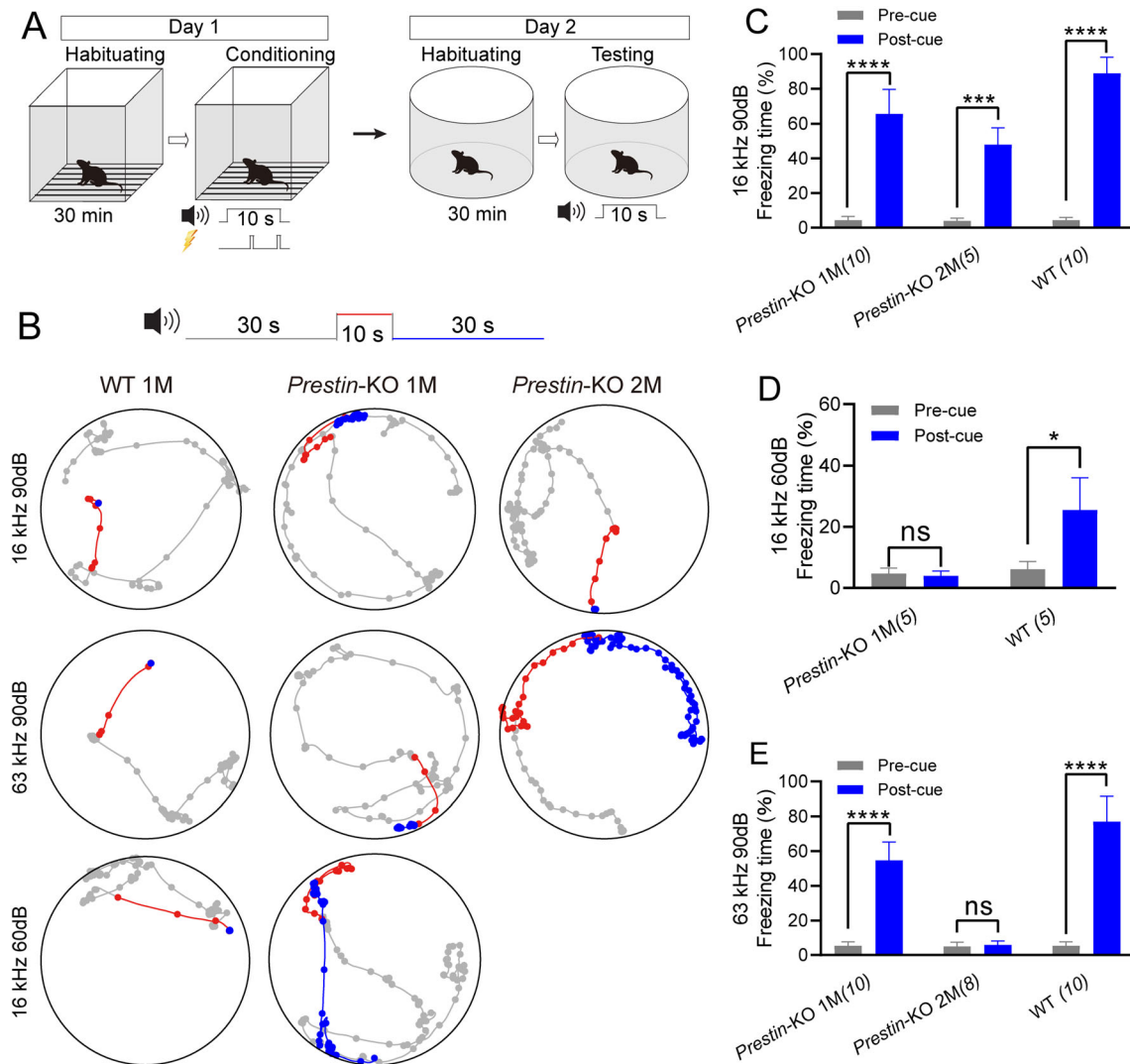
Fig. 2 Ultrahigh-frequency hearing-associated freezing behavior is preserved in 1-month-old (1M) *Prestin*-KO mice. **A** Paradigm of sound-cue associated freezing behavior. Pure-tone sound at 16 kHz or 63 kHz played by a TDT ES1 (Free Field) electrostatic speaker is used as the conditioned stimulus, and foot-shock was used as the unconditioned stimulus. **B** Representative examples of locomotion of control mice, 1-month (1M), and 2-month (2M) *Prestin-KO* mice before (gray, 30 s), during (red, 10 s), and after (blue, 30 s) the pure-tone sound cue. The mice had been trained to pair either the 16-kHz or the 63-kHz cue with the foot-shock-induced freezing. Dots indicate the location of a mouse every 0.5 s. Note that the 2M Prestin-KO mouse reacts to the 16 kHz but not the 63 kHz cue at 90 dB SPL.

C Percentage freezing time with the 16-kHz cue at 90 dB SPL. Pre-cue *vs* post-cue, paired *t*-test test, *Prestin*-KO 1-month (1M), $t_9 = 13.7$, ****$P < 0.0001$; *Prestin*-KO 2-month (2M), $t_4 = 9.477$, ***$P = 0.0009$; WT, $t_9 = 27.57$, ****$P < 0.0001$. **D** Percentage freezing time with the 16-kHz cue at 60 dB SPL. Pre-cue *vs* Post-cue, paired *t*-test test, *Prestin*-KO 1M, $t_4 = 1.0$, $P = 0.3739$; WT, $t_5 = 3.796$, *$P = 0.0127$. **E** Percentage freezing time with the 63-kHz cue at 90 dB SPL. Pre-cue *vs* Post-cue, paired *t*-test test, *Prestin*-KO 1M, $t_9 = 14.07$, ****$P < 0.0001$; *Prestin*-KO 2M, $t_7 = 0.7977$, $P = 0.4512$; WT, $t_9 = 15.81$, ****$P < 0.0001$. In (**C–E**), data are presented as the mean ± SD, and N numbers are shown in panels.

cells in 1.5-month *Prestin*-KO mice was not as profound as that in 2-month-old animals (Fig. 3E). *Prestin*-KO mice at the age of 1 month showed mostly preserved OHCs and IHCs, except for some OHC loss at very basal locations (Fig. 3B, F). Mechanistically, this may hinder the preservation of ultrahigh-frequency hearing (Fig. 1E). Further, we examined the cochleae from 3-week-old *Prestin*-KO mice and found that most of their hair cells were preserved (Fig. 3C, G). Thus, by measuring mABR thresholds in

3-week-old *Prestin*-KO mice (Fig. 4), we continued to show an obvious loss of hearing sensitivity at 4–32 kHz, as was seen in the 1-month-old *Prestin*-KO mice. Nevertheless, ultrasonic hearing in the range from 40 kHz to 80 kHz remained similar to the control cohort (Fig. 4C, D, gray *vs* yellow). These results from 3-week-old mice provide further confirmation that the Prestin defect disrupts lower frequency- but not ultrahigh-frequency hearing. The mABR thresholds of 3-week-old mice at ultrahigh

Fig. 3 Progressive loss of hair cells in *Prestin*-KO mice. **A** Reconstructed whole cochlear coil showing outer hair cell (OHC) survival from a 2-month-old (2M) *Prestin*-KO mouse. The cochlea is labeled with MYO7A antibody (white), phalloidin (red), and DAPI (blue). Left panels: scale bar, 300 μm. Right panels: enlarged images of apical, middle, and basal fragments in the dashed-line frames in (**A**). Scale bar, 100 μm. Note OHCs are only preserved in the apical coil. **B, C** Reconstructed whole cochlear coils showing OHC survival from a 1-month-old (1M) *Prestin*-KO mouse (**B**) and a 3-week-old (3W) *Prestin*-KO mouse (**C**). All the staining conditions are similar to (**A**). Note that most of the OHCs are present except in the basal part (**B**). **D–G** Loss of OHCs and IHCs in positions along the cochlear coil (as ratios) in 2M (**D**), 6W (**E**), 1M (**F**), and 3W (**G**) *Prestin*-KO mice. In (**D–G**), data are presented as the mean ± SD, and N numbers are shown in panels.
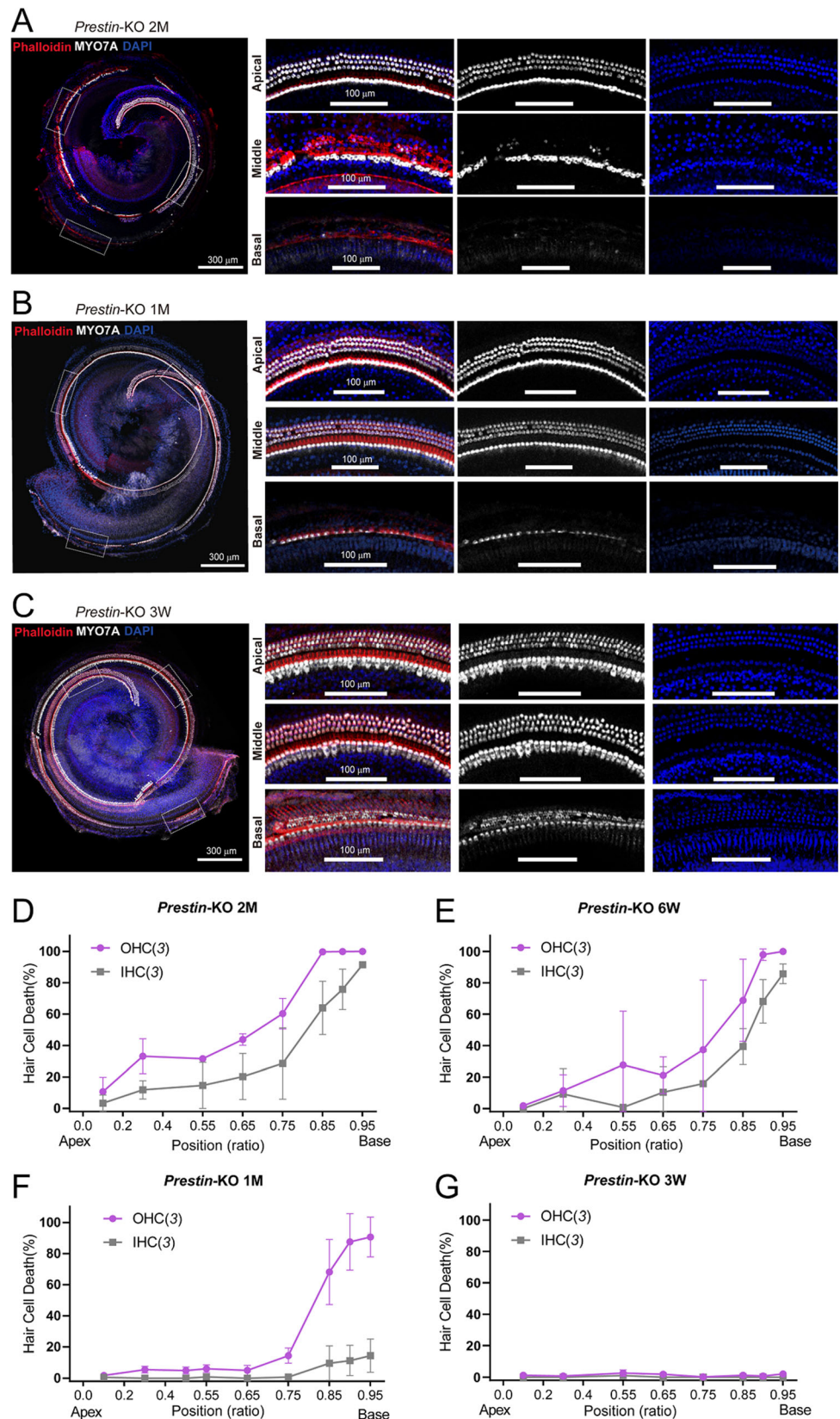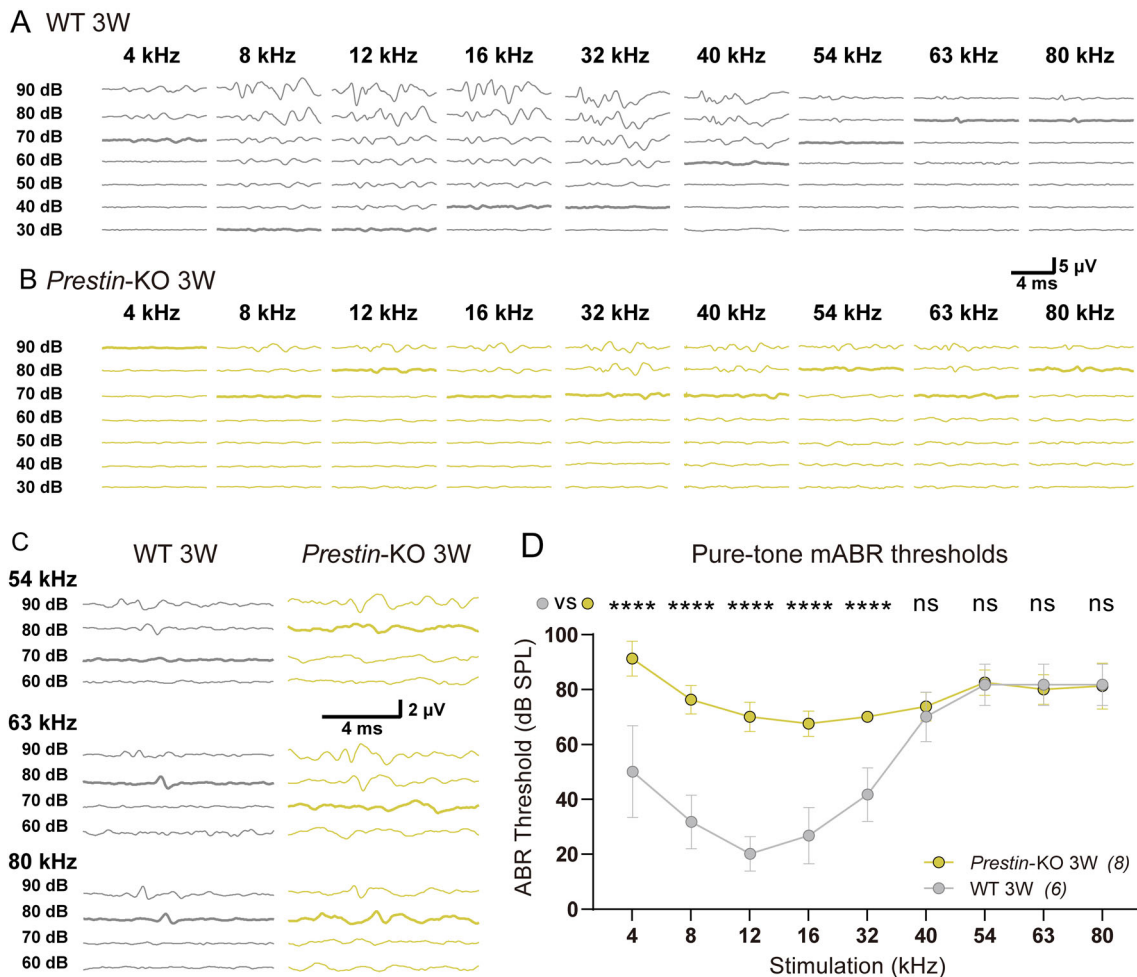
Fig. 4 mABR measurements from 3-week-old (3W) *Prestin*-knock-out mice. **A** Representative example of mABR signals in a 3W WT mouse. **B** Representative example of mABR signals in a 3W *Prestin*-KO mouse. **C** Amplified representative examples of mABR signals in response to 54–80 kHz, 60–90 dB SPL stimuli (visual thresholds bolded). The peak at ∼3 ms is used to identify the threshold. **D** Pure-tone mABR thresholds in *Prestin*-KO and control mice at 3W. Groups frequencies are compared at each frequency. *Prestin*-KO mice *vs* control mice, Sidak's multiple comparisons test, 4 kHz, ****P <0.0001; 8 kHz, ****P <0.0001; 12 kHz, ****P <0.0001; 16 kHz, ****P <0.0001; 32 kHz, ****P <0.0001; 40 kHz, P = 0.9824; 54 kHz, P >0.9999; 63 kHz, P >0.9999; 80 kHz, P >0.9999. Data are presented as the mean ± SD. N numbers are shown in panels.

frequencies were slightly higher than those of 1-month-old animals (Fig. 1E *vs* Fig. 4D), probably because ultrasonic hearing was not fully mature at 3 weeks of age.

Ultrahigh Frequency-induced Response in Cochlear OHCs After Prestin Deletion

As the cells responsible for cochlear amplification, OHCs possess mechano-electrical and electro-mechanical transducers (for functional forward and reverse transduction) at low frequencies, both of which are required for normal functionality. We examined both transductions, including ultrahigh-frequency transduction in *ex vivo* cochlea preparations. First, reverse transduction was tested with nonlinear capacitance (NLC) recordings, which showed complete loss of motility in *Prestin*-KO OHCs, but not in the control cohort (Fig. 5A, B). Next, we tested whether Prestin contributes to ultrahigh-frequency forward transduction at the cellular level. The OHCs were stimulated by ultrahigh-frequency vibration while responses were monitored using Ca^{2+} imaging of the hemicochlea with an epifluorescence microscope [31]. A custom-made *ex vivo* stimulation stage delivered vibration of 80 kHz, which mimicked mechanical vibration in the cochlea driven by ultrahigh frequency (Fig. 5C). The cochlea preparation was loaded with Fluo-8 AM, a sensitive Ca^{2+} dye, to illuminate the vibration-evoked Ca^{2+} response of the hair cells.

The major cell type that takes up Ca^{2+} dye, the OHCs in 1-month-old WT mice showed a significant increase in fluorescence when subjected to 80 kHz vibration (Fig. 5D, E). A similar ultrahigh-frequency-elicited Ca^{2+} response
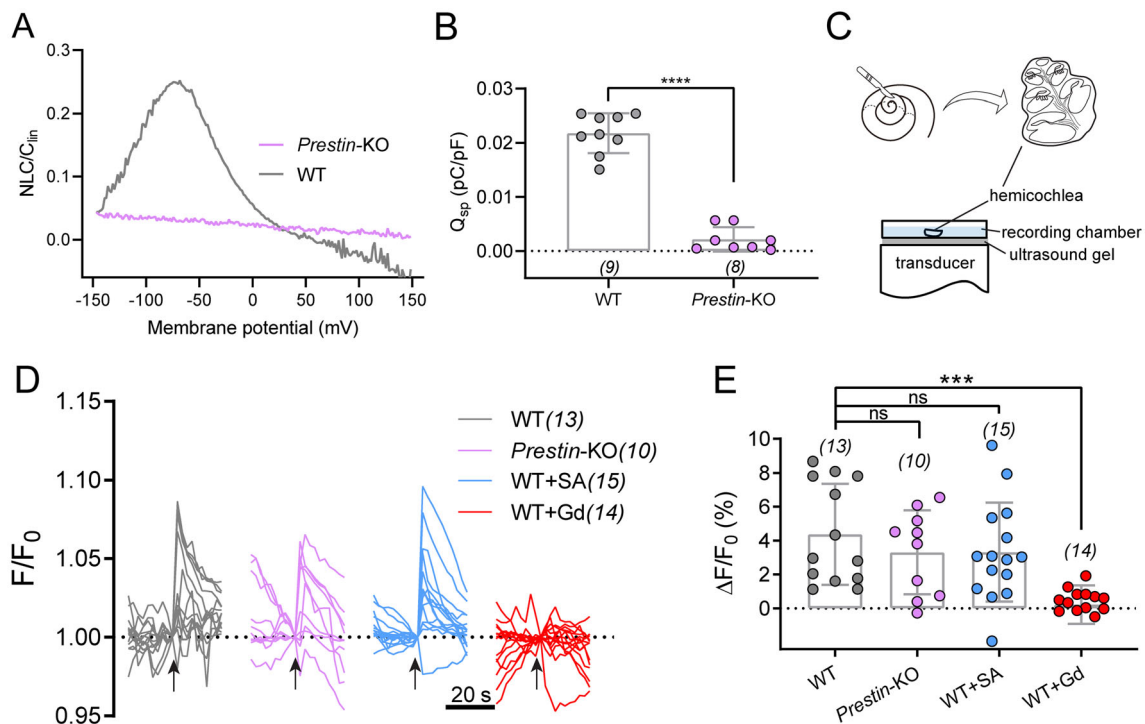
778

Neurosci. Bull. July, 2022, 38(7):769–784

Fig. 5 Ultrahigh-frequency-induced response in cochlear OHCs after Prestin deletion. **A** Nonlinear capacitance (NLC) in both *Prestin*-knockout and WT control OHCs. A representative example showing typical NLC pattern from a control OHC (gray). The NLC is absent in Prestin-knockout OHCs (purple). **B** Q_{sp} (Q_{max}/C_{lin}) in *Prestin*-KO and WT OHCs. Unpaired *t*-test, ****P <0.0001. **C** Schematic showing preparation of hemicochlea and setup for ultrasonic transducer stimulation. An 80-kHz transducer is fixed underneath the recording dish with ultrasound gel. **D** Ultrasonic stimulation evokes Ca^{2+} responses in OHCs of cochlea preparations from control and *Prestin*-KO mice. WT cochleae, *Prestin*-KO cochleae, WT cochleae treated with 10 mmol/L salicylic acid (WT+SA) were examined for the blockade of Prestin, and WT cochleae were treated with 10 μmol/L Gd^{3+} (WT+Gd). Arrows indicate ultrasonic stimulation. The images were collected at 2-s intervals. **E** Quantification of the peak Ca^{2+} responses of OHCs calculated from recordings in (**D**). Kruskal-Wallis test: WT *vs Prestin*-KO, P >0.9999; WT *vs* WT+SA, P >0.9999; WT *vs* WT+Gd, ***P = 0.0001. In (**B**) and (**E**), data are presented as the mean ± SD, and N numbers are shown in panels.

was recorded in WT OHCs, *Prestin*-KO OHCs, and WT OHCs when exposed to salicylic acid perfusion (10 mmol/L), which blocks Prestin function (Fig. 5D, E) [41]. Furthermore, this response was abolished by treatment with the non-selective cation channel blocker, Gd^{3+} (10 μmol/L) (Fig. 5D, E). In addition, low-frequency fluid-jet-induced hair-bundle mechanotransduction was preserved in *Prestin*-KO OHCs (Fig. S2). This result is similar to that seen in WT animals; inhibition by the mechanotransduction channel blocker dihydrostreptomycin (Fig. S2). These results suggest that Prestin is not responsible for ultrahigh-frequency forward transduction.

Salicylate Disrupts Low-frequency Hearing but not Ultrahigh-frequency Hearing

The OHC loss in *Prestin*-KO mice (Fig. 3) may compromise efforts to fully define the role of Prestin in ultrahigh-frequency hearing. To test this hypothesis more closely, we used pharmacological methods to acutely disrupt Prestin

function while maintaining OHC integrity. One-month-old WT mice were injected i.p. with salicylate to inhibit Prestin electromotility *in vivo* [42, 43]. The mABR thresholds were monitored every 10 min until 120 min after the thresholds stabilized, and were measured again on day 2 to test hearing recovery. Fig. 6A shows the mABR threshold-changes *vs* tone frequencies after salicylate injection. The threshold variation after salicylate injection is shown in Fig. 6B at a finer time resolution. Immediately after the injection, the 32–40 kHz thresholds were elevated. 70 min after injection, lower frequency thresholds (12–40 kHz) were elevated by ∼20 dB SPL and stabilized. In contrast, higher frequency thresholds (54–80 kHz) showed no significant change. The threshold elevation of 12–40 kHz recovered on the second day, indicating that the elevation was due to salicylate injection. These results indicate that the hearing sensitivity at lower frequencies (12–20 kHz) largely relies on Prestin electromotility, while sensitivity at higher frequencies (54–80 kHz) does not. It is interesting to note that 32–40 kHz thresholds showed different variation compared to lower and higher frequencies
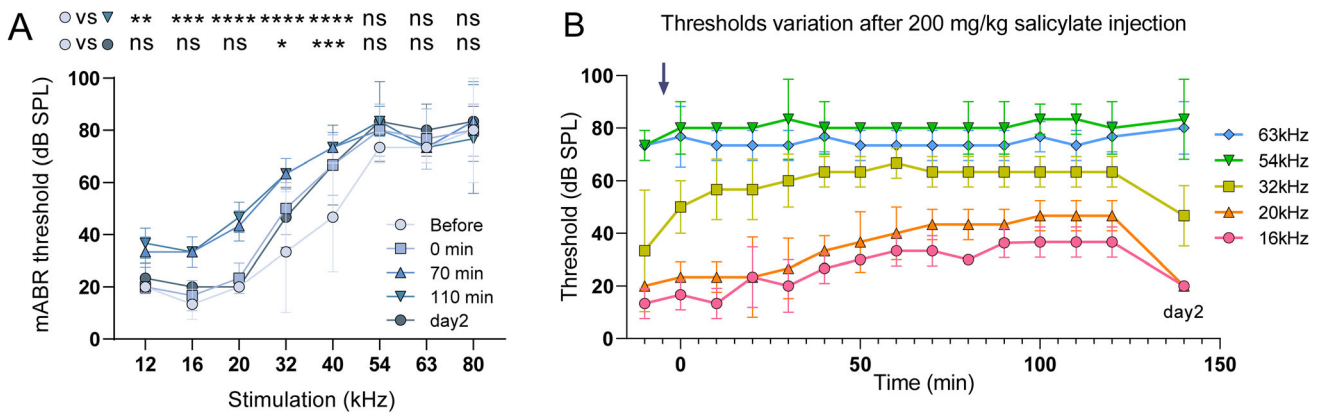
Fig. 6 Salicylate disrupts low-frequency hearing but not ultrahigh-frequency hearing. **A** Pure-tone mABR thresholds change after 200 mg/kg salicylate i.p. injection in 1-month-old C57BL/6 mice. Thresholds before the injection, just after the injection (0 min), and at 70 min, 110 min, one day (day 2) post-injection are shown. Thresholds at 12–20 kHz show significant elevation after injection and stabilize at 70 min post-injection. This elevation recovered on the second day. In contrast, 54–80 kHz thresholds remained unchanged. Before *vs* 110 min, Dunnett test, 12 kHz, **P = 0.0041; 16 kHz,

***P = 0.0005; 20 kHz, ****P <0.0001; 32 kHz, ****P <0.0001; 40 kHz, ****P <0.0001; 54 kHz, *P* = 0.1380; 63 kHz, *P* >0.9999; 80 kHz, *P* = 0.8995. Before *vs* day2, Dunnett test, 12 kHz, *P* = 0.8995; 16 kHz, *P* = 0.4577; 20 kHz, *P* >0.9999; 32 kHz, *P = 0.0280; 40 kHz, ***P = 0.0005; 54 kHz, *P* = 0.1380; 63 kHz, *P* = 0.4577; 80 kHz, *P* = 0.8995. **B** Time-lapse mABR threshold variation after salicylate injection. The injection time was defined as 0 min (gray arrow). Data are presented as the mean ± SD. *n* = 3.

(Fig. 6): the thresholds increased immediately after salicylate injection (0 min) and had not completely recovered to the untreated level by the second day. This may be due to salicylate-induced tinnitus, a known side-effect [44].

Prestin-DTR Mice Used for Selective OHC Ablation

The previous experiments with *Prestin*-knockout mice exposed to salicylate were designed to examine Prestin's role in ultrahigh-frequency hearing distinct from other OHC factors. Next, we investigated ultrahigh-frequency hearing in mice with OHC-specific ablation, using the DT/DTR system that has been applied successfully to kill cells of interest [45]. A *Prestin-P2A-DTR* knock-in mouse line was generated (*Prestin-DTR* mice), which exhibit *Prestin* promoter-driven DTR expression in its entirety, while preserving intact OHC Prestin expression [33]. After one injection of DT (20 ng/g) at postnatal day 21 (P21), the cochleae were dissected from heterozygous *Prestin-DTR/+* and littermate (+/+) control mice, at P28 (Fig. 7A). Compared to the DT-injected controls in which all hair cells were intact (Fig. 7B, D, E), injected *Prestin-DTR/+* mice showed OHC loss of ∼90% along the cochlear coils (Fig. 7C, D), in contrast to IHCs (Fig. 7C, E). This immunostaining result demonstrates the high efficiency of DT/DTR-driven OHC damage in *Prestin-DTR* mice.

Ultrahigh-frequency Hearing Is Disrupted in Prestin-DTR Mice

Using a similar injection procedure (as in Fig. 7A), we measured the mABR thresholds in the two mouse groups. Compared with the control littermate mice in the 4–80 kHz frequency range (Fig. 8A, C), mice with DTR-induced OHC loss showed significant elevation of the mABR threshold (Fig. 8B, C). This suggested that reduction in OHCs resulted in severe hearing loss over the entire frequency range. mABR audiograms showed two kinds of threshold elevation profile (Fig. 8C). For 4–40 kHz, the experimental mice retained residual hearing with thresholds ∼10 dB below 90 dB SPL (Fig. 8C, green). In line with previous reports, residual hearing capacity in this frequency range relies on intact IHCs when amplification is uniquely disrupted by a lack of OHC-based eM [17]. On the other hand, for 40–80 kHz frequencies, there were no detectable mABR thresholds to 90 dB SPL in *Prestin-DTR/+* mice (Fig. 8C, green). This indicates that there is more disrupted hearing sensitivity in ultrahigh frequencies. Moreover, it suggests that the loss of OHCs, rather than the lack of OHC eM, is the determining factor in abolishing ultrahigh-frequency sensitivity.

Next, sound-associated fear conditioning experiments were applied to assess hearing function in the *Prestin-DTR/+* mice and controls. Figure 8D shows an example of locomotion in injected experimental mice and littermate controls. Freezing behavior was quantified as the percentage of time that the mice stopped moving as a function of the fright response (Fig. 8E, F). With 16-kHz 90-dB SPL

Fig. 7 Cochlear OHC loss in DT-injected *Prestin-DTR* mice. **A** Schedule of DT injection and related tests. **B** Immunostaining image showing hair cell status in a control mouse at P28. Enlarged images show survival of OHCs in apical, middle, and basal locations. The cochlea is labeled with MYO7A antibody (white), phalloidin (red), and DAPI (blue). Note that most OHCs are lost but IHCs are not. Scale bar, 100 μm. **C** Immunostaining image showing hair cell status in a *Prestin-DTR* mouse at P28. The staining protocol and display conditions are as in (**B**). Scale bar, 100 μm. **D, E** Percentage loss of OHCs (**D**) and IHCs (**E**) at locations along the cochlea coil of P28 *Prestin-DTR* and control mice. N numbers are shown in panels.
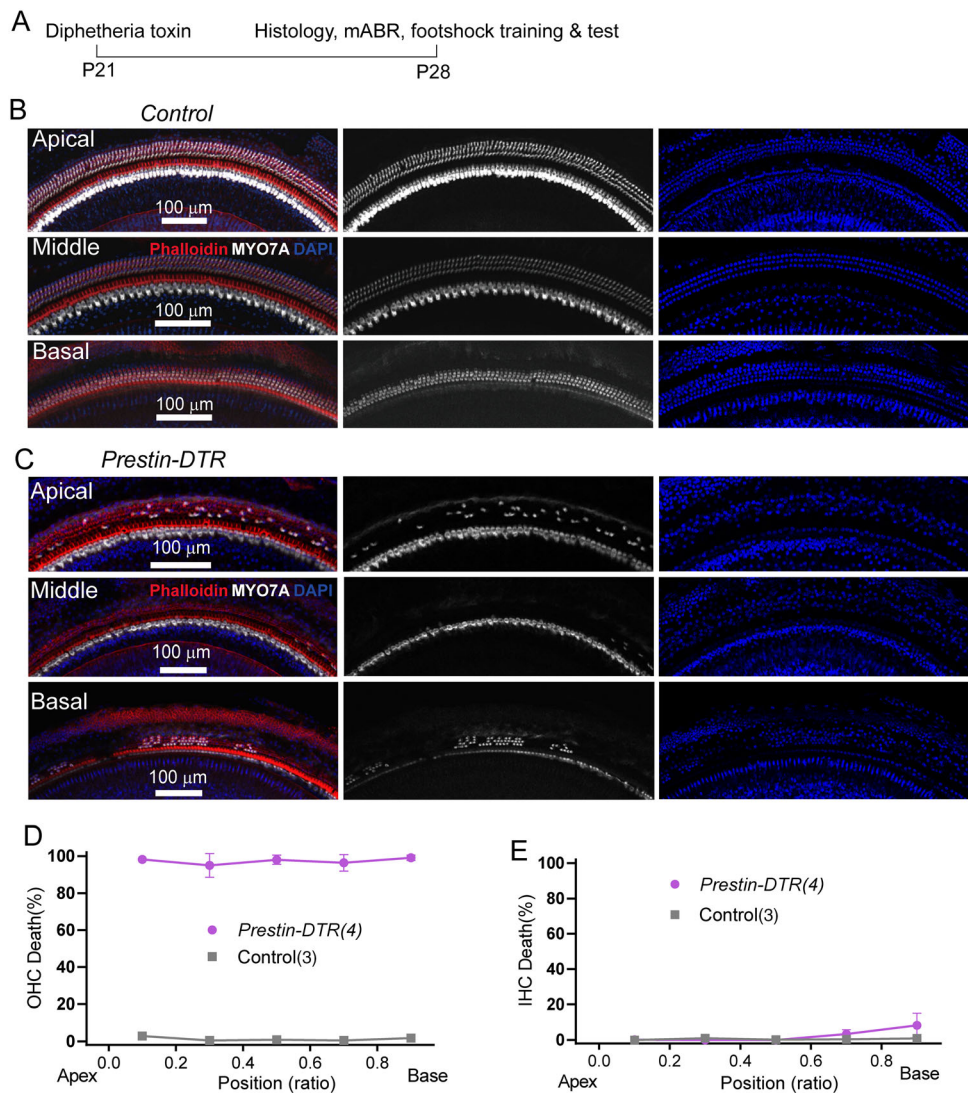
cues, control mice exhibited significantly different freezing times pre- and post-cue (Fig. 8E, right). However, *Prestin-DTR* mice showed no learning deficits with 16-kHz 90-dB SPL cues since freezing was preserved after DTR-induced OHC knockout (Fig. 8E, left). The stimulus at 90 dB SPL was used because it was higher than the hearing threshold at 16 kHz as demonstrated by mABR testing (Fig. 8E). Freezing time was slightly reduced in DTR-induced OHC-knockout mice due to hearing loss. The freezing behavior of control mice in response to 63-kHz 90-dB SPL cues was well preserved (Fig. 8F, right). In contrast, OHC-knockout mice lacked this behavior, as their freezing times for both pre- and post-sound cues were near 0% (Fig. 8F, left). These results, which complement the mABR data and behavioral data from *Prestin*-KO mice (Figs 1, 2, and), show that the presence and functionality of OHCs are essential for ultrahigh-frequency sound detection.

Discussion

In summary, we found that OHCs are essential for sensitive ultrahigh-frequency hearing. When OHCs were killed, either by DT/DTR-mediated cell toxicity in 1-month-old *Prestin-DTR* mice (Fig. 7C, D), or by extensive degeneration due to removal of Prestin in 2-month-old *Prestin*-KO mice (Fig. 3A, D), ultrahigh-frequency hearing (>40 kHz) was completely abolished. Our data suggest that Prestin is not essential for ultrahigh-frequency hearing, since ultrahigh-frequency hearing in 3-week-old *Prestin*-KO mice was preserved when Prestin was absent but OHCs were still present. These conclusions were supported by mABR recordings (Figs 1, 4, and 8A–C) and freezing behavior tests (Figs 2 and 8D–F).

By providing locally enhanced amplification, Prestin appears to improve frequency tuning [10, 16, 30]. This raises the question of how wide a hearing frequency range
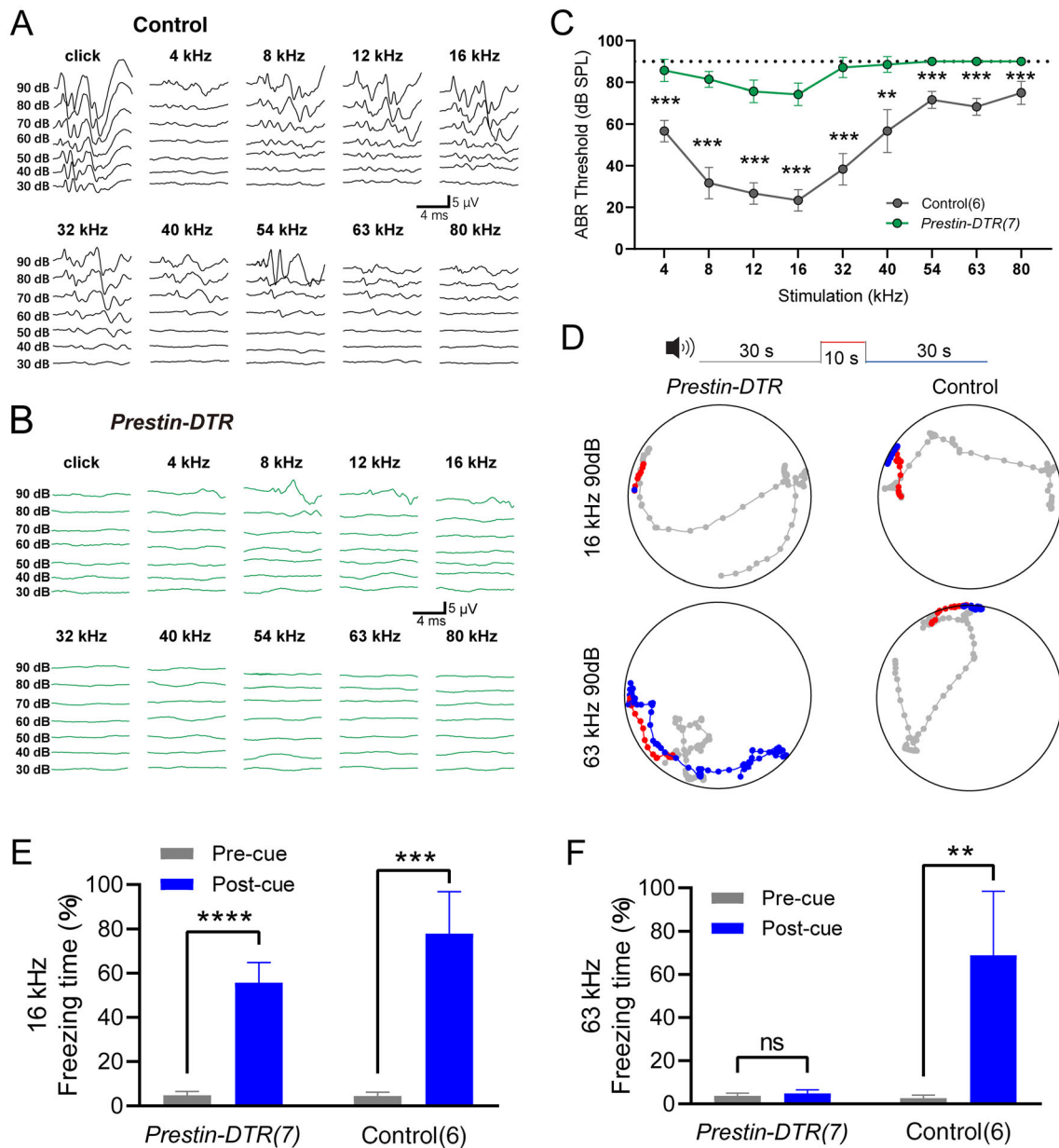
Fig. 8 mABR measurements and acoustically-associative freezing behavior of DT-injected *Prestin-DTR* mice. **A** Representative example of mABR signals in an injected littermate control mouse. **B** Representative example of mABR signals in an injected *Prestin-DTR/+* mouse. **C** mABR thresholds in the *Prestin-DTR/+* mice (green) and control littermate mice (without *Prestin-DTR* expression, dark gray). All mice were injected with DT. Note that the injected *Prestin-DTR/+* mice show no detectable mABR response at 90 dB SPL at frequencies from 54 kHz to 80 kHz. Control *vs* injected *Prestin-DTR/+*, Mann-Whitney test, **$P = 0.0012$ at 40 kHz, ***$P = 0.0006$ at other frequencies. **D** Representative examples of locomotion of control and *Prestin-DTR/+* mice before (gray, 30 s), during (red, 10 s), and after (blue, 30 s) the pure-tone sound cue at 90 dB SPL. The mice had been trained to pair either the 16-kHz or the 63-kHz cue with the foot-shock-induced freezing. Dots indicate the location of a mouse every 0.5 s. Injected littermate mice were used as controls. **E, F** Percentage freezing time with the 16-kHz cue (**E**) or the 63-kHz cue (**F**). Pre-cue *vs* Post-cue, paired *t*-test, *Prestin-DTR/+* mice at 16 kHz, $t_6 = 13.81$, ****$P < 0.0001$; Control mice at 16 kHz, $t_5 = 9.774$, ***$P = 0.0002$; *Prestin-DTR/+* mice at 63 kHz, $t_8 = 0.1187$, $P = 0.9094$; Control mice at 63 kHz, $t_5 = 5.386$, **$P = 0.003$. In (**C**), (**E**), and (**F**), data are presented as the mean $\pm$ SD. N numbers are shown in panels. All the mice were ~1 month old.

Prestin supports. Compound action potential (CAP) recordings have been used to probe the frequency-sensitivity in *Prestin*-KO mice [10, 46]. However, in these experiments, older mice (30–58 days) were used, and demonstrated a complete CAP threshold shift from a low- to higher-frequency (45 kHz) boundary of recordings. There is extensive OHC loss in mice older than 1 month [40], and two studies have shown further evidence of hearing

sensitivity and frequency selectivity in *Prestin*-KO mice (17–21 days old) [16, 30]. Interestingly, in *Prestin*-KO mice, the CAP thresholds were elevated at all frequencies from low to high (up to 70 kHz) [30], and basilar membrane displacement measured by interferometry showed that the tuning characteristic frequency shifted from 60 kHz to 45 kHz [16, 30]. Subsequently, data from *Prestin-499* mice that carry a motility-defect V499G point mutation, showed that *Prestin-499* mice completely lost sharp frequency tuning. This effect is similar to that reported in post-mortem studies [30], which argue that knockout of Prestin affects both the stiffness of OHCs and organ of Corti mechanics.

Furthermore, with phylogenetic analysis, Prestin shows an evolutionary correlation with echolocation [25–27, 29, 47]. The resulting membrane-conformation of prestin appears to be linked to its NLC function, which may participate in high-frequency hearing. In contrast, the combined experimental data from our investigations of *Prestin-DTR* mice and *Prestin*-KO mice provided evidence that distinguishes the role of Prestin from that of OHCs in frequency selectivity. For frequencies between 4 kHz and 32 kHz, 3-week- and 1-month-old *Prestin*-KO mice had audiometric thresholds and behavioral test results similar to 2-month-old *Prestin*-KO mice. This suggests that Prestin is essential for low-frequency hearing. However, at frequency ranges beyond 32 kHz, 3-week- and 1-month-old *Prestin*-KO mice showed hearing sensitivity similar to control mice, and this disappeared 2 months after OHCs died, indicating that OHC maintenance, not Prestin, is key to ultrahigh-frequency hearing.

In vivo recordings measuring the motion of the organ of Corti have provided insight into frequency selectivity in mice. However, due to *in vivo* experimental limitations, the cycle-by-cycle response of OHCs to high-frequency stimuli is hard to determine. Some authors have proposed that this is not a necessary requirement for the cochlear amplifier to operate [48]. A more recent study of organ of Corti motion patterns from the apical cochlea in mice show that the cycle-by-cycle response is enhanced by OHCs at frequencies <10 kHz, while this enhancement is reduced in *Prestin 499* mice [49]. Yet, it is still questionable how high the cut-off frequency of Prestin-based eM is supported by its molecular properties. Before Prestin was cloned [9], eM in guinea-pig OHCs was found to be responsive to stimulus frequencies beyond 79 kHz [23], or limited to the 22-kHz boundary [21]. However, these results were made in microchamber preparations that bypassed membrane filtering problems [50–52]. A whole-cell patch capacitance measurement approach revealed that the limiting frequency is near 25 kHz [22].

In vitro measurements of OHC electromotility and membrane filtering properties were made to bridge the gap between the experimental findings and the presumed theoretical barrier. By introducing the intrinsic piezoelectric property, it has been shown that the resistance–capacitance (RC) time constant is not a problem for high-frequency performance [53]. The RC time constant has been probed by assays ranging from an extracellularly-based cross-membrane voltage stimulus [21], to a robust K^+ current that drops membrane resistance, R_m [54], and subsurface cisternae resistance [55, 56]. It has been suggested that OHCs exhibiting a lower *in vivo* resting R_m and activating more ion channels, could, in theory, improve the RC time constant of the cell membrane [57]. However, NLC, the signature property of Prestin, seems to inhibit facilitation of the high-frequency eM response because peak NLC (nearly double the linear capacitance) slows the membrane time constant [56, 58, 59]. Recently, the membrane filtering issue has been revisited by simultaneous measurement of motility and NLC using both microchamber and whole-cell patch clamping techniques [19, 20]. With appropriate compensation of significant series resistance, the most optimistic estimation of the frequency-following capability for OHC electromotility does not exceed 16 kHz [60]. This is far below the known high-frequency hearing range in mammals, including humans. Due to the capacitive nature of the Prestin response, in order for eM to follow the cycle-by-cycle motion of the basilar membrane, the operation of Prestin needs to shift off the peak of the NLC curve. This shift is necessary to gain a slightly faster time constant at the expense of a lower contribution to mechanical input to organ of Corti movement [60, 61].

It should be noted that receptor potentials are driven by the opening and closing of the mechano-electrical transduction (MET) channels located at the tips of the stereocilia [62, 63]. Although MET channels have a super-fast activation time constant that is shorter than 10 μs (>100 kHz) [64], whether the bundle as a whole can overcome mechanical obstacles such as the viscoelastic drag of the fluid, and whether tectorial membrane coupling allows high-speed cyclical motion, remains an open question. These factors alone may exclude the possibility of Prestin-based eM in a cycle-by-cycle manner during ultrahigh-frequency stimulation. Thus, while benefiting from position-derived frequency selectivity, high-frequency OHCs may not require cycle-by-cycle motility. Rather, by using mechanics-based OHC-DC (Dieter's Cell) movement, or the mechanical properties inferred from the *in vivo* measurements taken by Vavakou *et al.*, high-frequency OHCs may serve as modulators for sound-evoked vibration [48].

In conclusion, our study has revealed that Prestin may not be an essential element for hearing at ultrahigh frequencies, the major frequency range for auditory

communication in mice. Prestin enhances the hearing sensitivity at low frequencies but is less likely to be an important biological factor in high-frequency hearing. Combined with our previous work [31], we speculate that the mechanosensitive channel PIEZO2 may acquire the ultrasonic energy and vibrate the cuticular plate, which further orchestrates the MET channel opening in hair bundles. Thus, Prestin enhances the sensitivity to low-to-middle-high frequencies by endowing OHCs with somatic motility, while PIEZO2 contributes to the detection of ultrahigh frequencies by vibrating stereocilia. Future work should recruit *in vivo* approaches, such as interferometry, to study organ of Corti motion patterns in more basal coil locations. This configuration would directly interrogate OHC motility across the cochlear coil upon hearing ultrahigh frequencies. Other genetically-engineered mouse models may be used, such as *Prestin-499* and conditional knockout of *Prestin*. For example, conditional knockout mice provide an excellent opportunity to examine the effect of Prestin deletion in adult animals that are known to have well-developed cochlear structure and the associated mechanical properties.

Conflict of interests The authors declare no competing interest.

References

1. Hopp SL, Owren MJ, Evans CS. Animal Acoustic Communication[M]. Berlin, Heidelberg: Springer Berlin Heidelberg, 1998.
2. Fettiplace R, Hackney CM. The sensory and motor roles of auditory hair cells. Nat Rev Neurosci 2006, 7: 19–29.
3. Ashmore J, Avan P, Brownell WE, Dallos P, Dierkes K, Fettiplace R. The remarkable cochlear amplifier. Hear Res 2010, 266: 1–17.
4. Hudspeth AJ. Integrating the active process of hair cells with cochlear function. Nat Rev Neurosci 2014, 15: 600–614.
5. Robles L, Ruggero MA. Mechanics of the mammalian cochlea. Physiol Rev 2001, 81: 1305–1352.
6. Ashmore J. Outer hair cells and electromotility. Cold Spring Harb Perspect Med 2019, 9: a033522.
7. Brownell WE, Bader CR, Bertrand D, de Ribaupierre Y. Evoked mechanical responses of isolated cochlear outer hair cells. Science 1985, 227: 194–196.
8. Ashmore JF. A fast motile response in guinea-pig outer hair cells: The cellular basis of the cochlear amplifier. J Physiol 1987, 388: 323–347.
9. Zheng J, Shen WX, He DZZ, Long KB, Madison LD, Dallos P. Prestin is the motor protein of cochlear outer hair cells. Nature 2000, 405: 149–155.
10. Dallos P, Wu XD, Cheatham MA, Gao JG, Zheng J, Anderson CT, *et al.* Prestin-based outer hair cell motility is necessary for mammalian cochlear amplification. Neuron 2008, 58: 333–339.
11. Schaechinger TJ, Gorbunov D, Halaszovich CR, Moser T, Kügler S, Fakler B, *et al.* A synthetic prestin reveals protein domains and molecular operation of outer hair cell piezoelectricity. EMBO J 2011, 30: 2793–2804.
12. Yamashita T, Hakizimana P, Wu S, Hassan A, Jacob S, Temirov J, *et al.* Outer hair cell lateral wall structure constrains the mobility of plasma membrane proteins. PLoS Genet 2015, 11: e1005500.
13. Bavi N, Clark MD, Contreras GF, Shen R, Reddy BG, Milewski W, *et al.* The conformational cycle of prestin underlies outer-hair cell electromotility. Nature 2021, 600: 553–558.
14. Butan C, Song Q, Bai J-P, Tan WJT, Navaratnam D, Santos-Sacchi J. 2021.
15. Ge JP, Elferich J, Dehghani-Ghahnaviyeh S, Zhao ZY, Meadows M, von Gersdorff H, *et al.* Molecular mechanism of prestin electromotive signal amplification. Cell 2021, 184: 4669-4679.e13.
16. Mellado Lagarde MM, Drexl M, Lukashkin AN, Zuo J, Russell IJ. Prestin's role in cochlear frequency tuning and transmission of mechanical responses to neural excitation. Curr Biol 2008, 18: 200–202.
17. Liberman MC, Gao JG, He DZZ, Wu XD, Jia SP, Zuo J. Prestin is required for electromotility of the outer hair cell and for the cochlear amplifier. Nature 2002, 419: 300–304.
18. Santos-Sacchi J. Reversible inhibition of voltage-dependent outer hair cell motility and capacitance. J Neurosci 1991, 11: 3096–3110.
19. Santos-Sacchi J. The speed limit of outer hair cell electromechanical activity. HNO 2019, 67: 159–164.
20. Santos-Sacchi J, Tan W. The frequency response of outer hair cell voltage-dependent motility is limited by kinetics of prestin. J Neurosci 2018, 38: 5495–5506.
21. Dallos P, Evans BN. High-frequency motility of outer hair cells and the cochlear amplifier. Science 1995, 267: 2006–2009.
22. Gale JE, Ashmore JF. An intrinsic frequency limit to the cochlear amplifier. Nature 1997, 389: 63–66.
23. Frank G, Hemmert W, Gummer AW. Limiting dynamics of high-frequency electromechanical transduction of outer hair cells. Proc Natl Acad Sci USA 1999, 96: 4420–4425.
24. Portfors CV, Perkel DJ. The role of ultrasonic vocalizations in mouse communication. Curr Opin Neurobiol 2014, 28: 115–120.
25. Li Y, Liu Z, Shi P, Zhang JZ. The hearing gene Prestin unites echolocating bats and whales. Curr Biol 2010, 20: R55–R56.
26. Liu Y, Rossiter SJ, Han XQ, Cotton JA, Zhang SY. Cetaceans on a molecular fast track to ultrasonic hearing. Curr Biol 2010, 20: 1834–1839.
27. Liu Z, Qi FY, Xu DM, Zhou X, Shi P. Genomic and functional evidence reveals molecular insights into the origin of echolocation in whales. Sci Adv 2018, 4: eaat8821.

28. Li G, Wang JH, Rossiter SJ, Jones G, Cotton JA, Zhang SY. The hearing gene Prestin reunites echolocating bats. Proc Natl Acad Sci U S A 2008, 105: 13959–13964.

29. Parker J, Tsagkogeorga G, Cotton JA, Liu Y, Provero P, Stupka E, et al. Genome-wide signatures of convergent evolution in echolocating mammals. Nature 2013, 502: 228–231.

30. Weddell TD, Mellado-Lagarde M, Lukashkina VA, Lukashkin AN, Zuo J, Russell IJ. Prestin links extrinsic tuning to neural excitation in the mammalian cochlea. Curr Biol 2011, 21: R682–R683.

31. Li J, Liu S, Song CM, Hu Q, Zhao ZK, Deng TT, et al. PIEZO2 mediates ultrasonic hearing via cochlear outer hair cells in mice. Proc Natl Acad Sci U S A 2021, 118: e2101207118.

32. Zhang H, Pan H, Zhou CY, Wei Y, Ying WQ, Li ST, et al. Simultaneous zygotic inactivation of multiple genes in mouse through CRISPR/Cas9-mediated base editing. Development 2018, 145: dev168906.

33. Sun SH, Li ST, Luo ZN, Ren MH, He SJ, Wang GQ, et al. Dual expression of Atoh1 and Ikzf2 promotes transformation of adult cochlear supporting cells into outer hair cells. Elife 2021, 10: e66547.

34. Romero S, Hight AE, Clayton KK, Resnik J, Williamson RS, Hancock KE, et al. Cellular and widefield imaging of sound frequency organization in primary and higher order fields of the mouse auditory cortex. Cereb Cortex 2020, 30: 1603–1622.

35. Garcia-Lazaro JA, Shepard KN, Miranda JA, Liu RC, Lesica NA. An overrepresentation of high frequencies in the mouse inferior colliculus supports the processing of ultrasonic vocalizations. PLoS One 2015, 10: e0133251.

36. Edge RM, Evans BN, Pearce M, Richter CP, Hu X, Dallos P. Morphology of the unfixed cochlea. Hear Res 1998, 124: 1–16.

37. Hu X, Evans BN, Dallos P. Direct visualization of organ of corti kinematics in a hemicochlea. J Neurophysiol 1999, 82: 2798–2807.

38. Edelstein A, Amodaj N, Hoover K, Vale R, Stuurman N. Computer control of microscopes using μManager. Curr Protoc Mol Biol 2010, Chapter 14: Unit14.20.

39. Liu S, Wang SF, Zou LZ, Li J, Song CM, Chen JF, et al. TMC1 is an essential component of a leak channel that modulates tonotopy and excitability of auditory hair cells in mice. Elife 2019, 8: e47441.

40. Wu XD, Gao JG, Guo YK, Zuo J. Hearing threshold elevation precedes hair-cell loss in prestin knockout mice. Mol Brain Res 2004, 126: 30–37.

41. Santos-Sacchi J. Control of mammalian cochlear amplification by chloride anions. J Neurosci 2006, 26: 3992–3998.

42. Oliver D, He DZ, Klöcker N, Ludwig J, Schulte U, Waldegger S, et al. Intracellular anions as the voltage sensor of prestin, the outer hair cell motor protein. Science 2001, 292: 2340–2343.

43. Stypulkowski PH. Mechanisms of salicylate ototoxicity. Hear Res 1990, 46: 113–145.

44. Lobarinas E, Sun W, Cushing R, Salvi R. A novel behavioral paradigm for assessing tinnitus using schedule-induced polydipsia avoidance conditioning (SIP-AC). Hear Res 2004, 190: 109–114.

45. Golub JS, Tong L, Ngyuen TB, Hume CR, Palmiter RD, Rubel EW, et al. Hair cell replacement in adult mouse utricles after targeted ablation of hair cells with diphtheria toxin. J Neurosci 2012, 32: 15093–15105.

46. Cheatham MA, Huynh KH, Gao J, Zuo J, Dallos P. Cochlear function in Prestin knockout mice. J Physiol 2004, 560: 821–830.

47. Marcovitz A, Turakhia Y, Chen HI, Gloudemans M, Braun BA, Wang HQ, et al. A functional enrichment test for molecular convergent evolution finds a clear protein-coding signal in echolocating bats and whales. Proc Natl Acad Sci U S A 2019, 116: 21094–21103.

48. Vavakou A, Cooper NP, van der Heijden M. The frequency limit of outer hair cell motility measured in vivo. Elife 2019, 8: e47667.

49. Dewey JB, Altoè A, Shera CA, Applegate BE, Oghalai JS. Cochlear outer hair cell electromotility enhances organ of Corti motion on a cycle-by-cycle basis at high frequencies in vivo. Proc Natl Acad Sci U S A 2021, 118: e2025206118.

50. Santos-Sacchi J. On the frequency limit and phase of outer hair cell motility: Effects of the membrane filter. J Neurosci 1992, 12: 1906–1916.

51. Housley GD, Ashmore JF. Ionic currents of outer hair cells isolated from the Guinea-pig cochlea. J Physiol 1992, 448: 73–98.

52. Ashmore J. Pushing the envelope of sound. Neuron 2011, 70: 1021–1022.

53. Spector AA, Brownell WE, Popel AS. Effect of outer hair cell piezoelectricity on high-frequency receptor potentials. J Acoust Soc Am 2003, 113: 453–461.

54. Ospeck M, Dong XX, Iwasa KH. Limiting frequency of the cochlear amplifier based on electromotility of outer hair cells. Biophys J 2003, 84: 739–749.

55. Halter JA, Kruger RP, Yium MJ, Brownell WE. The influence of the subsurface cisterna on the electrical properties of the outer hair cell. Neuroreport 1997, 8: 2517–2521.

56. Song L, Santos-Sacchi J. An electrical inspection of the subsurface cisternae of the outer hair cell. Biophys J 2015, 108: 568–577.

57. Johnson SL, Beurg M, Marcotti W, Fettiplace R. Prestin-driven cochlear amplification is not limited by the outer hair cell membrane time constant. Neuron 2011, 70: 1143–1154.

58. Song L, Santos-Sacchi J. Disparities in voltage-sensor charge and electromotility imply slow chloride-driven state transitions in the solute carrier SLC26a5. Proc Natl Acad Sci U S A 2013, 110: 3883–3888.

59. Santos-Sacchi J, Iwasa KH, Tan W. Outer hair cell electromotility is low-pass filtered relative to the molecular conformational changes that produce nonlinear capacitance. J Gen Physiol 2019, 151: 1369–1385.

60. Santos-Sacchi J, Tan W. Voltage does not drive prestin (SLC26a5) electro-mechanical activity at high frequencies where cochlear amplification is best. iScience 2019, 22: 392–399.

61. Santos-Sacchi J, Tan W. Complex nonlinear capacitance in outer hair cell macro-patches: effects of membrane tension. Sci Rep 2020, 10: 6222.

62. Beurg M, Fettiplace R, Nam JH, Ricci AJ. Localization of inner hair cell mechanotransducer channels using high-speed calcium imaging. Nat Neurosci 2009, 12: 553–558.

63. Russell IJ, Sellick PM. Tuning properties of cochlear hair cells. Nature 1977, 267: 858–860.

64. Peng AW, Ricci AJ. Glass probe stimulation of hair cell stereocilia. Methods Mol Biol 2016, 1427: 487–500.